

# Neutron Electric Dipole Moment and Tensor Charges from Lattice QCD

Tanmoy Bhattacharya,<sup>1,\*</sup> Vincenzo Cirigliano,<sup>1,†</sup> Rajan Gupta,<sup>1,‡</sup> Huey-Wen Lin,<sup>2,§</sup> and Boram Yoon<sup>1,¶</sup>  
(Precision Neutron-Decay Matrix Elements (PNDME) Collaboration)

<sup>1</sup>*Los Alamos National Laboratory, Theoretical Division T-2, Los Alamos, NM 87545*

<sup>2</sup>*Physics Department, University of California, Berkeley, CA 94720*

(Dated: June 16, 2022)

We present Lattice QCD results on the neutron tensor charges including, for the first time, a simultaneous extrapolation in the lattice spacing, volume, and light quark masses to the physical point in the continuum limit. We find that the “disconnected” contribution is smaller than the statistical error in the “connected” contribution. Our estimates in the  $\overline{\text{MS}}$  scheme at 2 GeV, including all systematics, are  $g_T^{d-u} = 1.020(76)$ ,  $g_T^d = 0.774(66)$ ,  $g_T^u = -0.233(28)$ , and  $g_T^s = 0.008(9)$ . The flavor diagonal charges determine the size of the neutron electric dipole moment (EDM) induced by quark EDMs that are generated in many new scenarios of CP-violation beyond the Standard Model (BSM). We use our results to derive model-independent bounds on the EDMs of light quarks and update the EDM phenomenology in split Supersymmetry with gaugino mass unification, finding a stringent upper bound of  $d_n < 4 \times 10^{-28} e \text{ cm}$  for the neutron EDM in this scenario.

PACS numbers: 11.15.Ha, 12.38.Gc

Keywords: neutron tensor charges, Lattice QCD, neutron EDM, split SUSY

Low energy precision measurements of neutron properties provide unique probes of new physics at the TeV scale. Searches for the neutron permanent EDM have high sensitivity to new BSM CP-violating interactions. Similarly, precision studies of correlations in neutron decay are sensitive to possible BSM scalar and tensor interactions. To fully realize the potential of the vibrant existing experimental neutron physics program [1], one needs to accurately calculate matrix elements of appropriate low-energy effective operators within neutron states. In this paper we describe lattice QCD calculations of the neutron tensor charges.

The flavor diagonal charges  $g_T^{u,d,s}$  are needed to quantify the contribution of the quark EDM to the neutron EDM and thus set bounds on BSM sources of CP violation. We find that the contribution of the “disconnected” diagrams to  $g_T^u$ ,  $g_T^d$  and  $g_T^s$  are small. Our results allow us to constrain split Supersymmetry models.

The isovector charge  $g_T^{d-u}$  is needed in the analysis of precision neutron  $\beta$ -decay. In Ref. [2] we showed that to complement experimental measurements of the helicity flip contributions to neutron  $\beta$ -decay at the precision of planned experiments ( $10^{-3}$  level), we need to calculate the iso-vector scalar and tensor charges,  $g_S^{d-u}$  and  $g_T^{d-u}$ , to about 10% accuracy. Results for  $g_T^{d-u}$  presented here meet the desired accuracy with control over all systematic errors, while  $g_S^{d-u}$  requires  $O(10)$  more statistics.

Details of the lattice QCD calculations are given in a companion paper [3]. Here we summarize the main points and focus on the results using nine ensembles of  $N_f = 2 + 1 + 1$  flavors of highly improved staggered quarks (HISQ) [4] generated by the MILC collaboration [5] and described in Table I. On these ensembles, we construct correlation functions using Wilson-clover fermions, as these preserve the continuum spin struc-

ture. To reduce short-distance noise, all lattices were “HYP” smeared [6]. Extensive tests were carried out on these nine HYP smeared ensembles to look for the presence of exceptional configurations [7], a possible problem with this mixed-action, Clover-on-HISQ, approach. None were detected. Issues of statistics, excited state contamination, operator renormalization, lattice volume, lattice spacing and the chiral behavior are detailed in [3].

The flavor diagonal neutron charges  $g_T^q$  are defined by  $\langle n(p, s) | \mathcal{O}_\Gamma^q | n(p, s) \rangle = g_T^q \bar{u}_s(p) \Gamma u_s(p)$ , with  $\mathcal{O}_\Gamma^q = \bar{q} \Gamma q$  and the spinors satisfying  $\sum_s u_s(\mathbf{p}) \bar{u}_s(\mathbf{p}) = (\not{p} + m)$ . The interpolating operator we use to create/annihilate the relativistically normalized neutron state  $|n(p, s)\rangle$  is  $\chi(x) = \epsilon^{abc} [q_1^{aT}(x) C \gamma_5 \frac{1}{2} (1 + \gamma_4) q_2^b(x)] q_1^c(x)$  with color indices  $\{a, b, c\}$ , charge conjugation matrix  $C$ , and  $q_1, q_2$  the two different flavors of light quark fields.

The zero-momentum projection of  $\chi(x)$  couples to the ground state, all radially excited states of the neutron, and multi-particle states. To reduce the coupling to radially excited states we Gaussian smear the quark fields in  $\chi(x)$ . To isolate the remaining excited state contamination, we include two states in the analysis of the two- and three-point functions at zero momentum [3]. Even though excited state contribution is exponentially suppressed, we were able to isolate the leading two unwanted matrix elements  $\langle 0 | \mathcal{O}_\Gamma | 1 \rangle$  and  $\langle 1 | \mathcal{O}_\Gamma | 1 \rangle$ , where  $|0\rangle$  and  $|1\rangle$  represent the ground and first excited neutron states. We find that the magnitude of  $\langle 0 | \mathcal{O}_\Gamma | 1 \rangle$  is about 16% of  $\langle 0 | \mathcal{O}_\Gamma | 0 \rangle$  and is determined with about 20% uncertainty on all the ensembles, whereas  $|\langle 1 | \mathcal{O}_\Gamma | 1 \rangle| \sim \langle 0 | \mathcal{O}_\Gamma | 0 \rangle$ , but has  $O(100\%)$  errors. As illustrated in Fig. 1 for the *a09m310* ensemble, the overlap of data in the center of the fit range for all the source-sink separations  $t_{\text{sep}}$  indicates that excited state contamination in the tensor charges is small and under control.

Ensemble ID		$a$ (fm)	$M_\pi^{\text{sea}}$ (MeV)	$M_\pi$ (MeV)	$L^3 \times T$	$M_\pi L$	$t_{\text{sep}}/a$	$N_{\text{conf}}$	$N_{\text{meas}}$
a12m310	□	0.1207(11)	305.3(4)	310.2(2.8)	$24^3 \times 64$	4.55	{8, 9, 10, 11, 12}	1013	8104
a12m220S	△	0.1202(12)	218.1(4)	225.0(2.3)	$24^3 \times 64$	3.29	{8, 10, 12}	1000	24000
a12m220	◇	0.1184(10)	216.9(2)	227.9(1.9)	$32^3 \times 64$	4.38	{8, 10, 12}	958	7664
a12m220L	▽	0.1189(09)	217.0(2)	227.6(1.7)	$40^3 \times 64$	5.49	10	1010	8080
a09m310	□	0.0888(08)	312.7(6)	313.0(2.8)	$32^3 \times 96$	4.51	{10, 12, 14}	881	7048
a09m220	◆	0.0872(07)	220.3(2)	225.9(1.8)	$48^3 \times 96$	4.79	{10, 12, 14}	890	7120
a09m130	○	0.0871(06)	128.2(1)	138.1(1.0)	$64^3 \times 96$	3.90	{10, 12, 14}	883	7064
a06m310	□	0.0582(04)	319.3(5)	319.6(2.2)	$48^3 \times 144$	4.52	{16, 20, 22, 24}	1000	8000
a06m220	◆	0.0578(04)	229.2(4)	235.2(1.7)	$64^3 \times 144$	4.41	{16, 20, 22, 24}	650	2600

TABLE I. The parameters of the (2+1+1) flavor HISQ lattices are quoted from Ref. [5]. The symbols used in plots are defined along with the ensemble ID. All chiral analyses are carried out with respect to the clover valence pion masses  $M_\pi$  which are tuned to be close to the Goldstone HISQ pion masses  $M_\pi^{\text{sea}}$ . We also give the source-sink separations ( $t_{\text{sep}}/a$ ) simulated, configuration analyzed ( $N_{\text{conf}}$ ) and the total number of measurements ( $N_{\text{meas}}$ ) made. Finite volume analysis is done in terms of  $M_\pi L$ .

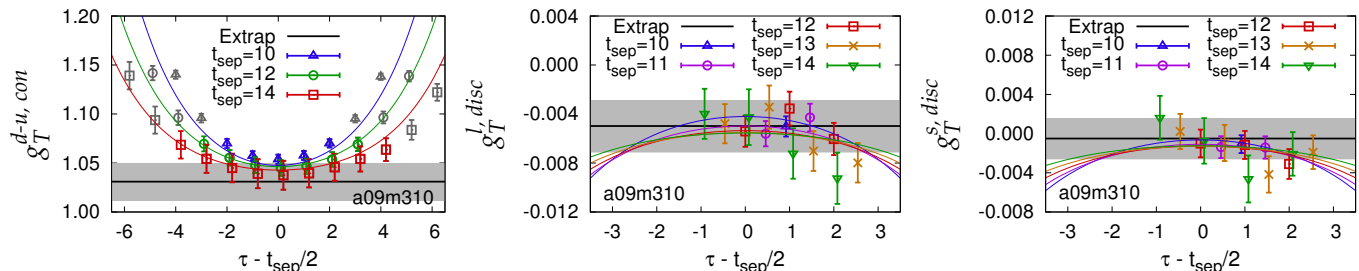


FIG. 1. Fits illustrating excited state contribution in the connected  $g_T^{d+u}$  and light and strange disconnected diagram for the  $a09m310$  ensemble. The data points represent  $g_T^a(\tau, t_{\text{sep}})$  obtained from calculations at different source-sink separations  $t_{\text{sep}}$  and operator insertion times  $\tau$ . The solid black line and the gray band are the ground state estimate and error.

The disconnected diagrams are estimated using a stochastic method accelerated with a combination of the truncated solver method (TSM) [8, 9], the hopping parameter expansion (HPE) [10, 11] and the all-mode-averaging (AMA) technique [12]. In most cases, the disconnected contribution is small and consistent with zero as illustrated in Fig. 1 for the  $a09m310$  ensemble. This feature was also observed in Ref. [13]. We find that the light quark contribution is too noisy to extrapolate to the continuum limit, so we do not include it in the central value. We, however, use the largest estimate, 0.0121, on the coarsest ensemble  $a12m310$  as an additional systematic error in  $g_T^d$ ,  $g_T^u$ , and  $g_T^{d+u}$ .

The renormalization factor, calculated non-perturbatively in the RI-sMOM scheme [14, 15] using the iso-vector operator, contributes a significant fraction of the total error. The charges converted into the  $\overline{\text{MS}}$  scheme at 2 GeV are given in Table II. We make a simultaneous fit to the data using the ansatz

$$g_T(a, M_\pi, L) = c_1 + c_2 a + c_3 M_\pi^2 + c_4 e^{-M_\pi L}. \quad (1)$$

where  $a$ ,  $M_\pi$ ,  $L$  are the lattice spacing, the pion mass, and the spatial lattice size. The data for all the tensor charges are essentially flat in these three variables; the intercept of the fit to  $g_T^{d+u}$  with the three planes is shown in Fig. 2. The final values for the renormalized neutron charges extrapolated to the physical point

( $M_\pi = 135$  MeV,  $a = 0$ ,  $M_\pi L = \infty$ ) are

$$\begin{aligned} g_T^d &= 0.774(66), & g_T^u &= -0.233(28), \\ g_T^{d+u} &= 1.020(76), & g_T^{d+u} &= 0.541(67). \end{aligned} \quad (2)$$

The  $\chi^2/\text{dof}$  for the fits are 0.1, 1.6, 0.4 and 0.2 respectively with  $\text{dof} = 5$ . Including the leading chiral logarithms [16] in Eq. (1) gives similar results [3].  $g_T^s$ , after extrapolation in the lattice spacing  $a$  and  $M_\pi^2$ , is

$$g_T^s = 0.008(9), \quad (3)$$

with a  $\chi^2/\text{dof} = 0.29$  with  $\text{dof} = 2$ . The intercept of the fit on the  $[g_T^s, a]$  plane is shown in Fig. 3.

Our result for  $g_T^{d+u}$ , with control over all systematic errors, is in good agreement with other lattice calculations [17, 18]. The LHPC [19] and RQCD [20] collaborations also find no significant dependence on the lattice spacing and volume, but do find a small dependence on the quark mass, so they extrapolate only in the quark mass using linear/quadratic (LHPC) and linear (RQCD) fits in  $M_\pi^2$ . Their final estimates,  $g_T^{d+u} = 1.04(2)$  (LHPC) and  $g_T^{d+u} = 1.005(17)$  (RQCD) are consistent with ours. A fit to our data versus only  $M_\pi^2$ , shown as an overlay in Fig. 2 (center), gives a similarly accurate estimate  $g_T^{d+u} = 1.059(29)$  with a  $\chi^2/\text{dof} = 0.3$ .

Our results on the tensor charges have implications for the neutron EDM and CP-violation in BSM theories. At

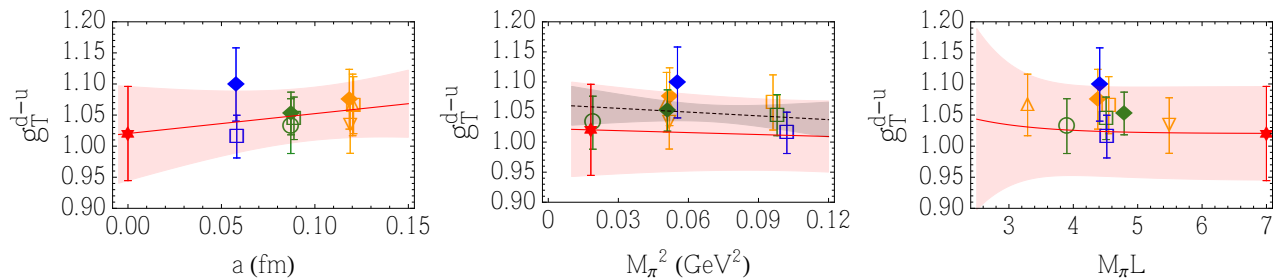


FIG. 2. A simultaneous fit of neutron  $g_T^{d-u}$  data versus  $a$ ,  $M_\pi^2$ , and  $M_\pi L$  using Eq. (1). The error band is shown as a function of each variable holding the other two at their physical value. The data are shown projected on to each of the three planes. The symbols are defined in Table I. The extrapolated value is marked by a red star. The gray band and the dashed line within it in the middle panel shows the fit versus  $M_\pi^2$  assuming no dependence on the other two variables.

Ensemble ID	$g_T^{\text{con},d}$	$g_T^{\text{con},u}$	$g_T^{\text{con},d-u}$	$g_T^{\text{con},d+u}$	$g_T^{\text{disc},l}$	$g_T^{\text{disc},s}$
a12m310	0.852(37)	-0.215(12)	1.066(46)	0.637(31)	-0.0121(23)	-0.0040(19)
a12m220S	0.857(43)	-0.209(19)	1.066(50)	0.649(44)	—	—
a12m220	0.860(40)	-0.215(15)	1.075(48)	0.644(36)	-0.0037(40)	-0.0010(27)
a12m220L	0.840(37)	-0.194(12)	1.033(45)	0.647(33)	—	—
a09m310	0.840(28)	-0.2051(98)	1.045(34)	0.634(25)	-0.0050(22)	-0.0005(21)
a09m220	0.836(28)	-0.216(10)	1.053(34)	0.619(25)	—	-0.0021(54)
a09m130	0.809(40)	-0.222(20)	1.032(44)	0.587(45)	—	—
a06m310	0.815(29)	-0.199(10)	1.015(34)	0.617(27)	-0.0037(65)	-0.0005(55)
a06m220	0.833(52)	-0.264(22)	1.099(59)	0.569(55)	—	—

TABLE II. Renormalized estimates of the connected ( $g_T^{\text{con}}$ ) and disconnected ( $g_T^{\text{disc}}$ ) contributions in the  $\overline{\text{MS}}$  scheme at 2 GeV.

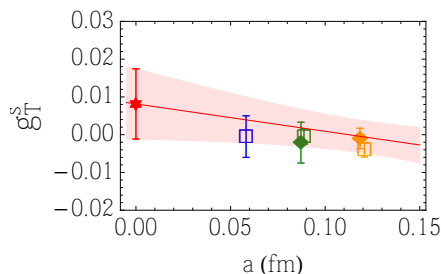


FIG. 3. The data for  $g_T^s$  and intercept of the fit versus  $a$  and  $M_\pi$  on the  $[g_T^s, a]$  plane. Notation is the same as in Fig. 2.

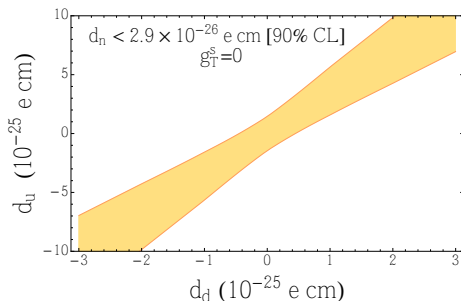


FIG. 4. Bounds on  $d_{u,d}$  with a  $1\sigma$  slab prior on  $g_T^u$  and  $g_T^d$  given in Eq. (2) and  $g_T^s = 0$ .

the hadronic scale,  $\mu \sim O(1)$  GeV, the dominant effect of new CP-violating couplings in BSM theories is encoded in local operators of dimension five and six. Leading, among them, are the elementary fermion EDMs [21, 22]:

$$\delta\mathcal{L}_{\text{CPV}} \supset -\frac{ie}{2} \sum_{f=u,d,s,e} d_f \bar{f} \sigma_{\mu\nu} \gamma_5 F^{\mu\nu} f. \quad (4)$$

The neutron EDM  $d_n$  depends on  $d_q$  as

$$d_n = g_T^u d_u + g_T^d d_d + g_T^s d_s, \quad (5)$$

consequently, improved knowledge of  $g_T^q$  combined with experimental bounds on  $d_n$  provides stringent constraints on new CP violation encoded in  $d_q$ . Note that we assume the Peccei-Quinn mechanism [23] and thus ignore the contribution of the QCD  $\Theta$ -term to nEDM.

Our calculation has the following impacts: (i) We reduce the uncertainty on  $g_T^{u,d}$  from the  $\sim 50\%$  of previous QCD sum rules (QCDSR) estimates [24] to the 10% level. (For a comparison of the lattice results with the Dyson-Schwinger [25] and other methods [26–29] see [3].) (ii) The central values of  $g_T^{u,d}$  are roughly 3/5 of the QCDSR and quark model estimates [24] widely used in phenomenological studies of BSM CP violation. (iii) Bounding the strangeness tensor charge  $g_T^s$  at the percent level is important for a large class of models in which  $d_q \propto m_q$  since  $m_s/m_d \sim 20$ . Our results imply that in such models  $g_T^s d_s$  may contribute up to 35% of the total  $d_n$  and the current  $O(1)$  fractional uncertainty in  $g_T^s$  gives rise to the largest uncertainty in  $d_n$ .

While, in general, BSM theories generate additional CP-violating operators in Eq. (4), there exist models in

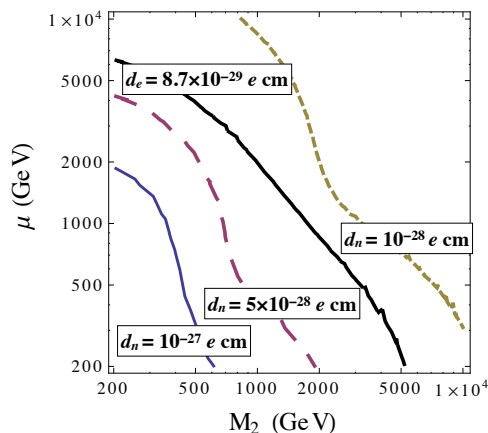


FIG. 5. Contour plots of  $d_n$  and  $d_e$  within split SUSY in the  $M_2$ - $\mu$  plane, assuming  $\sin \phi = 1$  and  $\tan \beta = 1$ .

which the fermion EDMs are the dominant sources of CP violation at low-energy, thus controlling the pattern of hadronic and atomic EDMs. In this case, using Eq. (5), our results on the tensor charges, and the experimental limit on the neutron EDM [30], we show 90% confidence level (CL) bounds on quark EDMs  $d_{u,d}$  in Fig. 4.

One notable scenario in which fermion EDM operators provide the dominant BSM source of CP violation is “split Supersymmetry (SUSY)” [31–33], in which all scalars, except for one Higgs doublet, are much heavier than the electroweak scale. This SUSY scenario achieves gauge coupling unification, has a dark matter candidate, and avoids the most stringent constraints associated with flavor and CP observables mediated by one-loop diagrams involving scalar particles. Contributions to fermion EDMs arise at two loops due to CP violating phases in the gaugino-Higgsino sector, while all other operators are highly suppressed [34]. To illustrate the impact of improved matrix elements in split SUSY, we use the analytic results and setup of Ref. [34], namely unified framework for gaugino masses at the GUT scale and a scalar mass  $\tilde{m} = 10^9$  GeV. The light fermion EDMs  $d_{e,u,d,s}$  depend on a single phase  $\phi$ , on  $\tan \beta$  [approximately through the overall factor  $\sin(\phi) \sin(2\beta)$ ] and on the gaugino ( $M_2$ ) and Higgsino ( $\mu$ ) mass parameters. Following Ref. [34] we set  $\tan \beta = 1$ ,  $\sin \phi = 1$  and present the results as contours in the  $M_2$ - $\mu$  plane, in the range between 200 GeV and 10 TeV.

Fig. 5 shows iso-level curves of  $d_n$  as well as the curve  $d_e = 8.7 \times 10^{-29}$  e cm, corresponding to the current 90% CL limit [35]. For the neutron EDM we use Eq. (5), evaluating both the  $d_q$ 's and the tensor charges at the scale  $\mu^{\overline{\text{MS}}} = 2$  GeV. Our result for  $d_n$  is appreciably smaller (factor of  $\sim 3$ ) than the one in Ref. [34]. We have traced back this difference to (i) our smaller values of the tensor charges compared to QCDSR [24]; (ii) different values for the light quark masses: we use the PDG [36] central value  $m_d(\overline{\text{MS}}, \mu = 2\text{GeV}) = 4.75$  MeV,

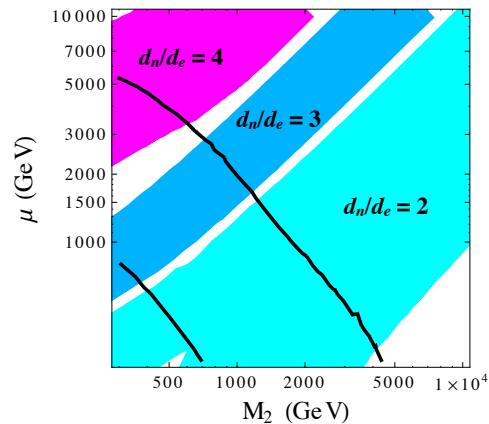


FIG. 6. Correlation between neutron and electron EDMs in split SUSY. The bands correspond to different values of  $d_n/d_e$  ( $\phi$ -independent). The thin solid lines correspond to  $d_e = 8.7 \times 10^{-29}$  e cm for  $\sin \phi = 1$  (outer curve) and  $\sin \phi = 0.2$  (inner curve).

while the value corresponding to the quark condensate used in Ref. [34] is larger,  $m_d(\overline{\text{MS}}, \mu = 1\text{GeV}) \approx 9$  MeV.

In Refs. [34, 37], it was pointed out that the strong correlation between electron and neutron EDM would provide a valuable experimental test of split SUSY. To investigate this further, in Fig. 6 we present bands corresponding to different values of  $d_n/d_e$  in the  $M_2$ - $\mu$  plane, the thickness of the bands reflects the behavior of  $d_n/d_e[M_2, \mu]$  and the uncertainty induced by the tensor charges, dominated by  $g_T^s$ . The fact that we can draw disconnected bands for  $d_n/d_e = 2, 3, 4$  is a welcome consequence of our reduced uncertainties in  $g_T^q$ : using the QCDSR input, each band would be as thick as the whole plot, giving essentially no discrimination.

Finally, based on the current 90% CL limit on  $d_e$ , we derive an upper limit for the neutron EDM in split SUSY. By maximizing the ratio  $d_n/d_e$  along the iso-level curves  $d_e = 8.7 \times 10^{-29}$  e cm corresponding to  $\sin \phi \leq 1$ , allowing  $g_T^q$  to vary in the lattice QCD ranges, we arrive at  $d_n < 4 \times 10^{-28}$  e cm<sup>1</sup>. Therefore, observation of the neutron EDM between the current limit of  $3 \times 10^{-26}$  e cm [30] and  $4 \times 10^{-28}$  e cm would falsify the split-SUSY scenario with gaugino mass unification.

We thank the MILC Collaboration for providing the 2+1+1 flavor HISQ lattices used in our calculations. Simulations were carried out on computer facilities of (i) the USQCD Collaboration, which are funded by the Office of Science of the U.S. Department of Energy, (ii) the Extreme Science and Engineering Discovery Environment (XSEDE), which is supported by National Science Foundation grant number ACI-1053575, (iii) the National

<sup>1</sup> Note that with QCDSR matrix elements, the split-SUSY upper bound would be less stringent, namely  $d_n < 1.2 \times 10^{-27}$  e cm.

Energy Research Scientific Computing Center, a DOE Office of Science User Facility supported by the Office of Science of the U.S. Department of Energy under Contract No. DE-AC02-05CH11231; and Institutional Computing at Los Alamos National Lab. The calculations used the Chroma software suite [38]. This material is based upon work supported by the U.S. Department of Energy, Office of Science of High Energy Physics under contract number DE-KA-1401020 and the LANL LDRD program. The work of HWL was supported by DOE grant No. DE-FG02-97ER4014. We thank Emanuele Mereghatti, Saul Cohen and Anosh Joseph for extensive discussions.

---

\* tanmoy@lanl.gov  
 † cirigliano@lanl.gov  
 ‡ rajan@lanl.gov  
 § hueywenlin@lbl.gov  
 ¶ boram@lanl.gov

- [1] D. Dubbers and M. G. Schmidt, *Rev.Mod.Phys.* **83**, 1111 (2011), arXiv:1105.3694 [hep-ph].
- [2] T. Bhattacharya, V. Cirigliano, S. D. Cohen, A. Filipuzzi, M. Gonzalez-Alonso, *et al.*, *Phys.Rev.* **D85**, 054512 (2012), arXiv:1110.6448 [hep-ph].
- [3] T. Bhattacharya, V. Cirigliano, S. Cohen, R. Gupta, A. Joseph, H.-W. Lin, and B. Yoon, (2015), in Preparation.
- [4] E. Follana *et al.* (HPQCD Collaboration, UKQCD Collaboration), *Phys.Rev.* **D75**, 054502 (2007), arXiv:hep-lat/0610092 [hep-lat].
- [5] A. Bazavov *et al.* (MILC Collaboration), *Phys.Rev.* **D87**, 054505 (2013), arXiv:1212.4768 [hep-lat].
- [6] A. Hasenfratz and F. Knechtli, *Phys.Rev.* **D64**, 034504 (2001), arXiv:hep-lat/0103029 [hep-lat].
- [7] T. Bhattacharya, S. D. Cohen, R. Gupta, A. Joseph, H.-W. Lin, *et al.*, *Phys.Rev.* **D89**, 094502 (2014), arXiv:1306.5435 [hep-lat].
- [8] S. Collins, G. Bali, and A. Schafer, *PoS LAT2007*, 141 (2007), arXiv:0709.3217 [hep-lat].
- [9] G. S. Bali, S. Collins, and A. Schafer, *Comput.Phys.Commun.* **181**, 1570 (2010), arXiv:0910.3970 [hep-lat].
- [10] C. Thron, S. Dong, K. Liu, and H. Ying, *Phys.Rev.* **D57**, 1642 (1998), arXiv:hep-lat/9707001 [hep-lat].
- [11] C. Michael, M. Foster, and C. McNeile (UKQCD collaboration), *Nucl.Phys.Proc.Suppl.* **83**, 185 (2000), arXiv:hep-lat/9909036 [hep-lat].
- [12] T. Blum, T. Izubuchi, and E. Shintani, *Phys.Rev.* **D88**, 094503 (2013), arXiv:1208.4349 [hep-lat].
- [13] A. Abdel-Rehim, C. Alexandrou, M. Constantinou, V. Drach, K. Hadjiyiannakou, *et al.*, *Phys.Rev.* **D89**, 034501 (2014), arXiv:1310.6339 [hep-lat].
- [14] G. Martinelli, C. Pittori, C. T. Sachrajda, M. Testa, and A. Vladikas, *Nucl.Phys.* **B445**, 81 (1995), arXiv:hep-lat/9411010 [hep-lat].
- [15] C. Sturm, Y. Aoki, N. Christ, T. Izubuchi, C. Sachrajda, *et al.*, *Phys.Rev.* **D80**, 014501 (2009), arXiv:0901.2599 [hep-ph].
- [16] J. de Vries, R. Timmermans, E. Mereghetti, and U. van Kolck, *Phys.Lett.* **B695**, 268 (2011), arXiv:1006.2304 [hep-ph].
- [17] S. Syritsyn, *PoS LATTICE2013*, 009 (2014), arXiv:1403.4686 [hep-lat].
- [18] M. Constantinou, *PoS LATTICE2014*, 001 (2014), arXiv:1411.0078 [hep-lat].
- [19] J. Green, J. Negele, A. Pochinsky, S. Syritsyn, M. Engelhardt, *et al.*, *Phys.Rev.* **D86**, 114509 (2012), arXiv:1206.4527 [hep-lat].
- [20] G. S. Bali, S. Collins, B. Glssle, M. Gckeler, J. Najjar, *et al.*, *Phys.Rev.* **D91**, 054501 (2015), arXiv:1412.7336 [hep-lat].
- [21] J. Engel, M. J. Ramsey-Musolf, and U. van Kolck, *Prog.Part.Nucl.Phys.* **71**, 21 (2013), arXiv:1303.2371 [nucl-th].
- [22] M. Pospelov and A. Ritz, *Annals Phys.* **318**, 119 (2005), arXiv:hep-ph/0504231 [hep-ph].
- [23] R. Peccei and H. R. Quinn, *Phys.Rev.Lett.* **38**, 1440 (1977).
- [24] M. Pospelov and A. Ritz, *Phys.Rev.* **D63**, 073015 (2001), arXiv:hep-ph/0010037 [hep-ph].
- [25] M. Pitschmann, C.-Y. Seng, C. D. Roberts, and S. M. Schmidt, *Phys.Rev.* **D91**, 074004 (2015), arXiv:1411.2052 [nucl-th].
- [26] A. Bacchetta, A. Courtoy, and M. Radici, *JHEP* **1303**, 119 (2013), arXiv:1212.3568 [hep-ph].
- [27] M. Anselmino, M. Boglione, U. D'Alesio, S. Melis, F. Murgia, *et al.*, *Phys.Rev.* **D87**, 094019 (2013), arXiv:1303.3822 [hep-ph].
- [28] Z.-B. Kang, A. Prokudin, P. Sun, and F. Yuan, *Phys.Rev.* **D91**, 071501 (2015), arXiv:1410.4877 [hep-ph].
- [29] Z.-B. Kang, A. Prokudin, P. Sun, and F. Yuan, (2015), arXiv:1505.05589 [hep-ph].
- [30] C. Baker, D. Doyle, P. Geltenbort, K. Green, M. van der Grieten, *et al.*, *Phys.Rev.Lett.* **97**, 131801 (2006), arXiv:hep-ex/0602020 [hep-ex].
- [31] N. Arkani-Hamed and S. Dimopoulos, *JHEP* **0506**, 073 (2005), arXiv:hep-th/0405159 [hep-th].
- [32] G. Giudice and A. Romanino, *Nucl.Phys.* **B699**, 65 (2004), arXiv:hep-ph/0406088 [hep-ph].
- [33] N. Arkani-Hamed, S. Dimopoulos, G. Giudice, and A. Romanino, *Nucl.Phys.* **B709**, 3 (2005), arXiv:hep-ph/0409232 [hep-ph].
- [34] G. Giudice and A. Romanino, *Phys.Lett.* **B634**, 307 (2006), arXiv:hep-ph/0510197 [hep-ph].
- [35] J. Baron *et al.* (ACME), *Science* **343**, 269 (2014), arXiv:1310.7534 [physics.atom-ph].
- [36] K. Olive *et al.* (Particle Data Group), *Chin.Phys.* **C38**, 090001 (2014).
- [37] S. Abel and O. Lebedev, *JHEP* **0601**, 133 (2006), arXiv:hep-ph/0508135 [hep-ph].
- [38] R. G. Edwards and B. Joo (SciDAC Collaboration, LHPC Collaboration, UKQCD Collaboration), *Nucl.Phys.Proc.Suppl.* **140**, 832 (2005), arXiv:hep-lat/0409003 [hep-lat].